J Mater Sci (2008) 43:989–1001
DOI 10.1007/s10853-007-2245-y

Electrical conduction behavior and immittance analysis of Gd and Mn substituted strontium titanate

Prakash Singh · Prabhakar Singh · Sindhu Singh · Om Parkash · Devendra Kumar

Received: 3 April 2007 / Accepted: 22 October 2007 / Published online: 15 November 2007
© Springer Science+Business Media, LLC 2007

Abstract Various compositions in the system $Sr_{1-x}Gd_xTi_{1-x}Mn_xO_3$ ($x \leq 0.50$) were synthesized by solid-state ceramic route. Solid solution forms in all the compositions investigated. Crystal structure remains cubic up to $x = 0.10$ similar to $SrTiO_3$, while for compositions with $x \geq 0.30$, it becomes orthorhombic, similar to $GdMnO_3$. Average grain size is small in all the compositions investigated, and it decreases with increasing x. For compositions with $x \leq 0.30$, Seebeck coefficient is initially positive. It becomes negative at higher temperatures. For $x = 0.50$, it is negative over the entire temperature range of measurements. Immittance analysis shows the presence of two polarization processes, one due to grains and other due to grain boundaries. Results of DC resistivity, ρ_{dc} and Seebeck coefficient, α as a function of temperature show that in the samples with $x \leq 0.30$, in the lowest temperature range conduction occurs due to hopping of holes among Mn^{+3} and Mn^{4+} ions, and for $x = 0.50$ it occurs due to hopping of electrons among Mn^{2+} and Mn^{3+} ions over the entire temperature range. In the intermediate temperature range, for $x \leq 0.30$ the conduction occurs by hopping of electrons among Mn^{2+} and Mn^{3+} ions. For $x = 0.01$ and 0.05 conduction occurs due to diffusion of oxygen ions through doubly positively charged oxygen vacancies in the highest temperature range.

P. Singh · S. Singh · O. Parkash (✉) · D. Kumar
Department of Ceramic Engineering, Institute of Technology, Banaras Hindu University, Varanasi 221005, India
e-mail: opec_itbhu2003@yahoo.co.in

P. Singh
School of Sciences, Indira Gandhi National Open University, Maidan Garhi, New Delhi 110068, India

Introduction

In recent years, strontium titanate has attracted much attention due to its fascinating properties. Beside its relevance for electronics, sensor science, electrochemistry and photochemistry, $SrTiO_3$ is an excellent model material for a mixed-type conductor because of availability of a detailed knowledge of its defect models, chemical and transport parameters. Substitutions in $SrTiO_3$ modify its properties and promotes its use in electronic devices [1, 2]. Its conductivity can be easily controlled from n-type semiconductor to metallic conduction by Nb or La doping [3]. Manganese-doped $SrTiO_3$ has been investigated for its use as a functional ceramic by impregnating the grain boundaries with Mn [4–6]. Co-doped $SrTiO_3$, i.e., $Sr^{2+}_{1-y}Y^{3+}_y(Ti_{1-x}M_x)O_3$ ($x \neq y$), where M = Fe, Co, Ni, Mn, etc., has been studied for its possible application as an anode material in high-temperature solid electrolyte (HTSE) fuel cells [7]. One of the requirements for application as an anode material is that it should exhibit mixed ionic electronic conduction (MIEC). Y^{3+}, doped at Sr^{2+} site, acts as a donor to provide electrons as charge carriers, while acceptor doping of Fe, Co, Ni and Mn at Ti^{4+} site provides oxygen vacancies, $V_o^{\bullet\bullet}$. We have recently reported the synthesis, structure and electrical behavior of internally valence compensated system $Sr_{1-x}La_xTi_{1-x}Mn_xO_3$ ($x \leq 0.50$) prepared by solid-state method [8]. It has been found that resistivity decreases with increasing x. Composition with $x = 0.10$ seems to have potential as anode material in high-temperature solid electrolyte fuel cells.

As the size of rare earth ion decreases with increasing atomic number from lanthanum (La) to lutetium (Lu), the basicity of rare earth ion increases which leads to their competition for π electrons of oxygen ions involved in M–O

(Ti in this case) bonding. This would decrease covalency of M–O bonding, increasing localized character of *d* electrons [9]. This would influence the electrical and dielectric properties of the resulting material. To study the effect of rare earth ion on the electrical behavior, in the present work we attempted to synthesize a few samples in the co-doped system $Sr_{1-x}Gd_xTi_{1-x}Mn_xO_3$ ($x \leq 0.50$) to investigate the possibility of solid solution formation by solid-state route and study their crystal structure, microstructure and electron transport properties employing immittance analysis. Here Gd^{+3} ions because of their higher basicity would tend to compete for π electrons of M–O bonding and may influence its electrical and dielectric properties. Results of these investigations are reported in this work.

Experimental

Compositions with $x = 0.01$, 0.05, 0.10, 0.30 and 0.50 in the system $Sr_{1-x}Gd_xTi_{1-x}Mn_xO_3$ have been synthesized by solid-state ceramic route. Appropriate amounts of strontium carbonate, gadolinium oxalate, titanium dioxide and manganese carbonate, all of purity greater than 99.5%, (by mole) for all the above-mentioned compositions were weighed and mixed in a ball mill using agate jars and agate grinding media for 6 h using acetone as a mixing medium. The dried powders were calcined at 1,473 K in air for 12 h and then furnace cooled. Calcined powders were compacted under an optimum load of 70 KN in the form of cylindrical discs (dia. 12 mm) using 2% solution of PVA as binder. The pellets were slowly heated to 873 K and then held at this temperature for 1 h to burn off the binder. Thereafter, the temperature was raised to 1,573 K and the pellets were sintered in air at this temperature for 12 h. The sintered pellets were reground, pelletized and sintered at 1,573 K once again for 12 h to improve the chemical homogeneity of the product.

The sintered pellets were ground and powder X-ray diffraction patterns (XRD) were recorded using a Rigaku X-ray Diffractometer employing Cu-K_α radiation with a Ni filter. For microstructural studies, sintered pellets were polished using emery paper of grades 1/0, 2/0, 3/0, 4/0 and 5/0 successively followed by polishing on a velvet cloth with diamond paste of the order of 1 and 1/4 μm. These pellets were washed using distilled water followed by methanol. Then, these were etched chemically. The etchant used was 10 mL of 10 % HCl containing 2–3 drops of HF. Chemically etched pellets were washed with distilled water and coated with gold by sputtering technique. The micrographs were recorded using JEOL PSM 800 scanning electron microscope (SEM).

Seebeck coefficient was measured relative to platinum in the temperature range (600–1,000 K) in air on thick pellets of thickness ~7 mm. Escort EDM 3150 Multimeter was used to record voltage. For DC resistivity measurements, the samples were polished and electrode coated using Ag-Pd alloy paint which was matured by heating at 1,073 K for 20 min. The resistance was measured by a two-probe method in the temperature range 300–1,000 K using Keithley 616 Electrometer at steady temperatures.

The dielectric parameters and AC conductance were measured in the temperature range 150–500 K in a locally fabricated cell using programmed Novocontrol a-S High-Resolution Dielectric Analyser.

AC conductivity was calculated by the relation:

$$\sigma_{ac} = \frac{G \times d}{A} (\text{Ohm cm})^{-1} \quad (1)$$

where σ_{ac} is the AC conductivity, d is the thickness (in cm), G is the conductance and A is the area (in sq. cm) of the sample.

The values of real and imaginary parts of impedance, i.e., Z' and Z'' were calculated using the formula:

$$Z' = \frac{1}{\left[G\left(1 + \frac{1}{D^2}\right)\right]} \quad (2)$$

and

$$Z'' = \frac{Z'}{D} \quad (3)$$

where D is the dissipation factor.

Using these values of Z' and Z'', the real and imaginary components of modulus (M' and M'') were calculated as:

$$M' = \omega C_0 Z'', \ \omega = 2\pi f \quad (4)$$

$$M'' = \omega C_0 Z' \quad (5)$$

where f is the frequency and C_0 the capacitance of the empty cell used to house the materials and it depends on the geometry.

Results and discussion

All the compositions with $x = 0.01$, 0.05, 0.10, 0.20, 0.30 and 0.50 have been found to be single-phase solid solutions. XRD patterns for the different solid solution compositions are shown in Fig. 1(a–e). Formation of single phase was confirmed on the basis of absence of the characteristic lines of the constituent oxides or the other compounds among them in the powder X-ray diffraction patterns. X-ray diffraction data of all the compositions with $x \leq 0.10$ have been indexed on the basis of a cubic unit cell similar to $SrTiO_3$, while for compositions with $x = 0.30$ and 0.50, XRD data have been indexed on the basis of an orthorhombic unit cell similar to $GdMnO_3$. Lattice parameters were determined using a program 'CEL' and are given in Table 1.

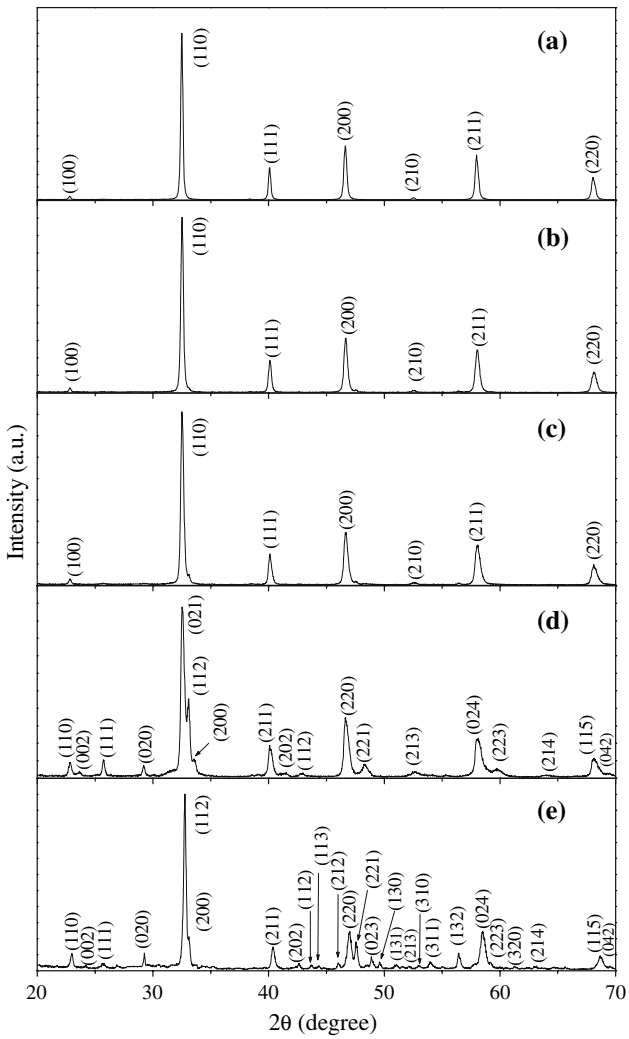

Fig. 1 XRD patterns for various compositions with x (**a**) 0.01, (**b**) 0.05, (**c**) 0.10, (**d**) 0.30, and (**e**) 0.50 in the system $Sr_{1-x}Gd_xTi_{1-x}Mn_xO_3$

The bulk density was calculated using Archimedes Principle. Theoretical density was calculated from the molecular weight of the formula unit and unit cell volume (Å^3). Percentage porosities were determined using the theoretical and experimental density. It was found that bulk density for various samples was greater than 90% of theoretical value. Percentage porosity decreases (i.e., sinterability increases) with increasing x. Lattice parameters, structure, unit cell volume, theoretical density, experimental density and percentage porosity for all the compositions are given in Table 1.

Scanning electron micrographs of the chemically etched surfaces of pellets coated with Au for different compositions are shown in Fig. 2. It is noted from Fig. 2 that for all the compositions, the microstructure is homogeneous with fine grain structure. The grains are nearly spherical in shape. It is observed that submicrometer-size grains coalesce during sintering forming bigger grains. The average grain size has been determined by linear intercept method. The average grain size is given in the Table 1. It has been found that the average grain size is <1 μm for all the compositions. The small grain size may be due to segregation of dopants at the grain boundaries which inhibit grain growth [10, 11]. Because of almost similar grain size in different compositions, its effect on their electrical behavior will be almost same.

It is observed from Fig. 3 that α remains constant over a small temperature range for the samples with $x \leq 0.10$ followed by a decrease with increasing temperature over the remaining temperature range of measurements. For $x = 0.20$ (not shown) and 0.30, it decreases slightly with increasing temperature, becomes negative above a particular temperature beyond which it becomes temperature independent. The sample with $x = 0.50$ exhibits negative but temperature-independent value over the entire temperature range.

Plots of logarithm of DC resistivity, log ρ_{dc} (ohm cm.) versus 1,000/T (K^{-1}) are shown in Fig. 4. For all the compositions, resistivity decreases with increasing temperature. For $x = 0.01$ and 0.05 these plots show two linear regions, whereas only one linear region is observed for $x \geq 0.10$. This shows that resistivity in these regions obey Arrhenius relationship according to equation

$$\rho_{dc} = \rho_0 \exp(E_a/kT) \quad (6)$$

where E_a is the activation energy for conduction. It is observed that in all the samples α decreases in the lower

Table 1 Composition, structure, lattice parameter, experimental density, % porosity and average grain size of different compositions in the system $Sr_{1-x}Gd_xTi_{1-x}Mn_xO_3$

Composition	Structure	Lattice Parameter (Å)			Theoretical density (gm/cm^3)	Experimental density (gm/cm^3)	% Porosity	Average Grain Size (μm)
		a	b	c				
$x = 0.01$	Cubic	3.8930	–	–	5.186	4.663	10	<1
$x = 0.05$	Cubic	3.8892	–	–	5.288	4.781	9	<1
$x = 0.10$	Cubic	3.8905	–	–	5.391	4.943	8	<1
$x = 0.30$	Orthorhombic	5.3144	5.8108	7.4620	5.952	5.471	8	<1
$x = 0.50$	Orthorhombic	5.3826	5.8079	7.4023	6.367	5.891	7	<1

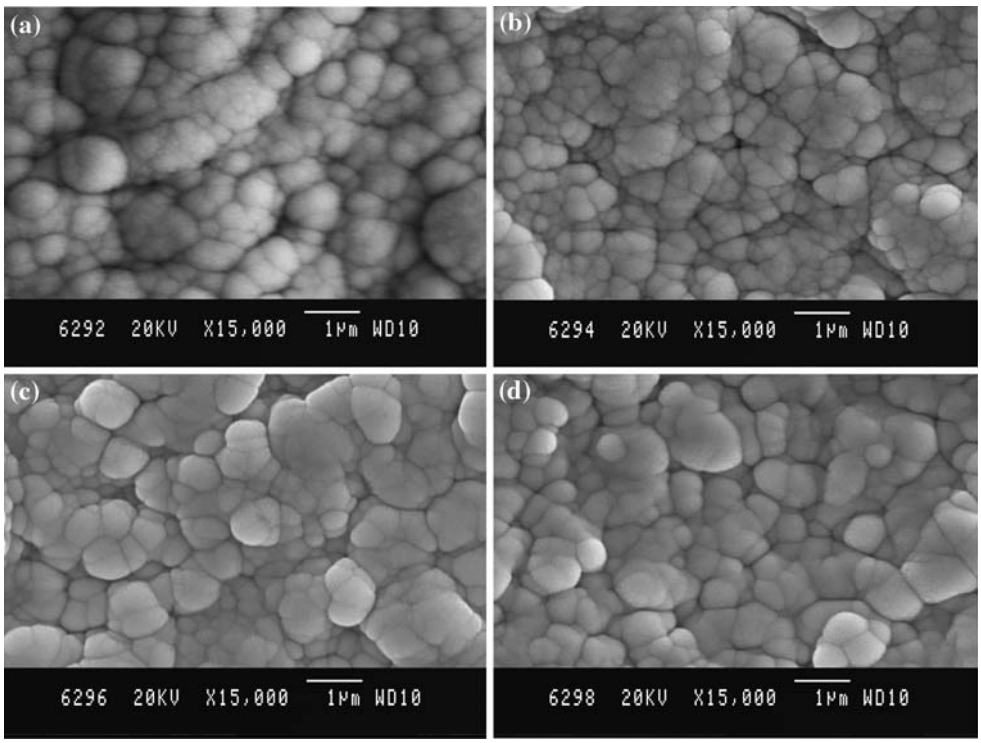

Fig. 2 Scanning electron micrographs (SEM) of chemically etched surfaces of compositions with x (**a**) 0.01, (**b**) 0.05, (**c**) 0.10, and (**d**) 0.30 in the system $Sr_{1-x}Gd_xTi_{1-x}Mn_xO_3$

temperature range for $0.10 \leq x \leq 0.30$ and then becomes constant at higher temperature. Resistivity decreases with increasing temperature over the entire temperature range.

Values of activation energies in different temperature regions obtained by least square fitting of the data are given in Table 2. The values of activation energy, E_a, of conduction decrease with increasing concentration of Gd and Mn, i.e., x. Activation energy in the higher temperature region is higher as compared to the low-temperature region for both the compositions with $x = 0.01$ and 0.05. For compositions with $x = 0.01$ and 0.05, it is interesting to note that the change in slope of $\log \rho_{dc}$ versus $1{,}000/T$ curves occurs around the same temperature where α starts decreasing (Fig. 3).

Results of Electron paramagnetic resonance (EPR) spectra of these materials (figure not shown) show that most of Mn ions are in +3 states. A small concentration (less than 10% of the substituted concentration, i.e., x) of Mn may be in +2 and +4 states also. The following possibilities exist for incorporation of Mn ions on Ti^{4+} sites

$$2SrO + Mn_2O_3 \xrightarrow{SrTiO_3} 2Sr_{Sr}^{\times} + 2Mn_{Ti}' + V_O^{\bullet\bullet} + 5O_O \quad (7)$$

$$2SrO + 2MnO \xrightarrow{SrTiO_3} 2Sr_{Sr}^{\times} + 2Mn_{Ti}'' + 2V_O^{\bullet\bullet} + 4O_O \quad (8)$$

$$2SrO + Mn_2O_3 + \frac{1}{2}O_2 \xrightarrow{SrTiO_3} 2Sr_{Sr}^{\times} + 2Mn_{Ti}' + 2h^{\bullet} + 6O_O \quad (9)$$

$$2SrO + 2MnO + O_2 \xrightarrow{SrTiO_3} 2Sr_{Sr}^{\times} + 2Mn_{Ti}'' + 4h^{\bullet} + 6O_O \quad (10)$$

Here all the species are written in accordance with Kröger Vink notation of defects. Besides the above reactions, there may be slight loss of oxygen at high temperature during sintering [12, 13] in accordance with the reaction

$$O_O \Leftrightarrow \frac{1}{2}O_2 + V_O^{\bullet\bullet} + 2e' \quad (11)$$

Moos et al. [14] and Moos and Härdtl [15] in their experiments have shown that the oxygen vacancies in $SrTiO_3$ exist in singly ionized state at room temperature. With increasing temperature, they ionize according to the reaction:

$$V_O^{\bullet} \Leftrightarrow V_O^{\bullet\bullet} + e' \quad (12)$$

Undoped $SrTiO_3$ exhibit p-type conduction when prepared in air atmosphere. This has been explained due to higher concentration of acceptor impurities in the starting raw materials as compared to donor impurities due to relative more abundance of acceptors in nature [16].

When both gadolinium and manganese are substituted in equimolar amount in $SrTiO_3$, charge compensation may take place internally as given below:

$$Gd_2O_3 + Mn_2O_3 \xrightarrow{SrTiO_3} 2Gd_{Sr}^{\bullet} + 2Mn_{Ti}' + 6O_O \quad (13)$$

assuming all Mn ions exist in +3 oxidation state.

This should not lead to any significant change in the conductivity. The nature of conduction changes from p-type to n-type with increasing temperature and x (Fig. 3). It means that complete internal charge compensation does not take place as per Eq. 13. Compositions with $x \leq 0.10$ exhibit p-type conductivity over a certain temperature

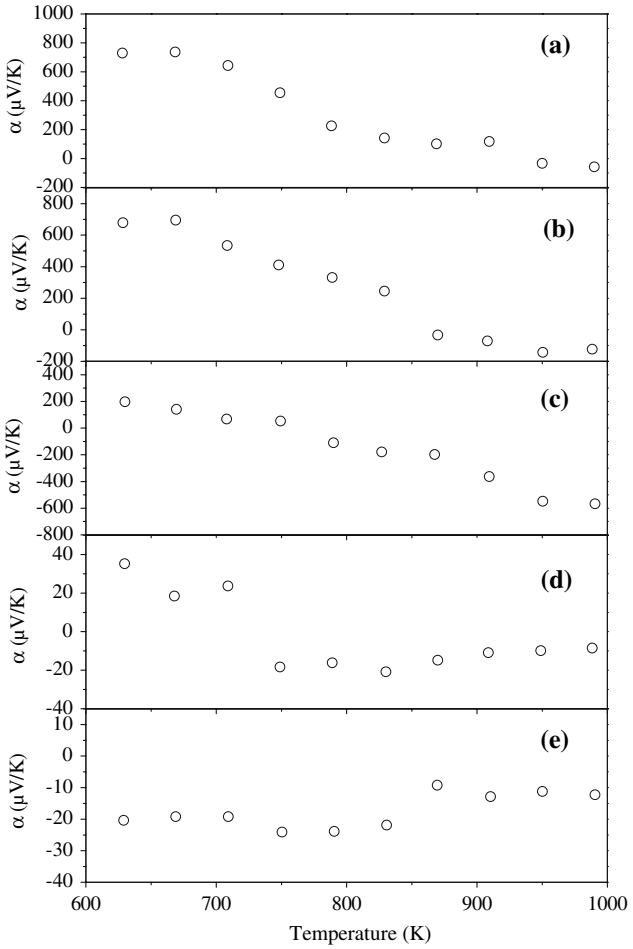

Fig. 3 Variation of Seebeck coefficient α with temperature for compositions with x (**a**) 0.01, (**b**) 0.05, (**c**) 0.10, (**d**) 0.30, and (**e**) 0.50 in the system $Sr_{1-x}Gd_xTi_{1-x}Mn_xO_3$

range due to greater concentration of acceptor impurities in the starting materials as explained above. But these materials also contain singly and doubly positively charged oxygen vacancies, viz. $V_O^{\bullet}$ and $V_O^{\bullet\bullet}$ as mentioned above due to rapid or non-equilibrium cooling of the specimen after sintering. $V_O^{\bullet}$ give rise to energy levels 0.2–0.3 eV below the conduction band [17]. They ionize as per Eq. 12 generating electrons. These electrons may be captured by Mn^{3+} ions to produce Mn^{2+} ions. Therefore, concentration of Mn^{2+} ions increases with increasing temperature. Above a particular temperature, their concentration becomes higher than that of Mn^{4+} ions. So the conduction is dominated by hopping of electrons among Mn^{2+} and Mn^{3+} ions, giving rise to n-type conductivity.

$SrTiO_3$ is a wide-band gap semiconductor with a band gap ~3.2–3.4 eV [18, 19]. The value of activation energy for diffusion of oxygen ions in undoped $SrTiO_3$ at and above 1,000 K has been reported to be 1.0–1.2 eV [16]. Similarly activation energy of conduction, E_a, for grains and grain boundaries determined by admittance

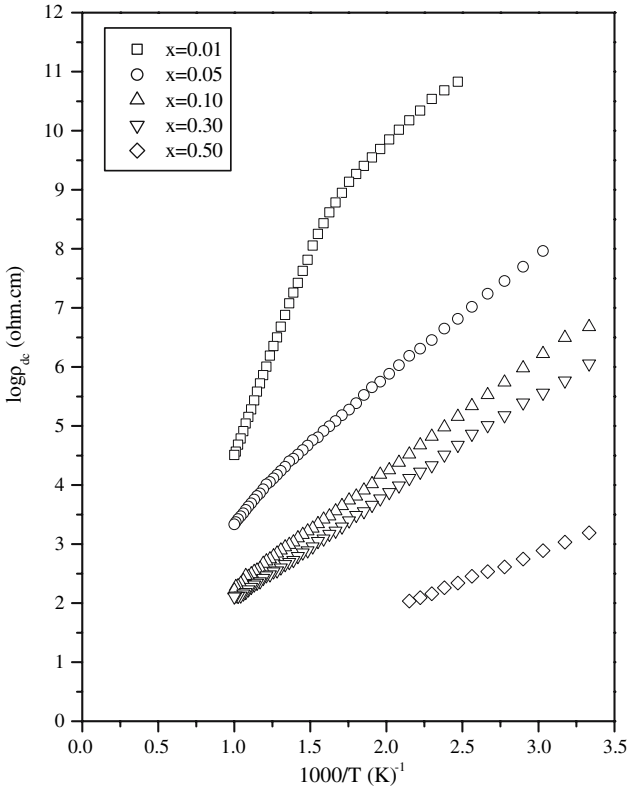

Fig. 4 Variation of log ρ_{dc} with inverse of temperature for different compositions x in the system $Sr_{1-x}Gd_xTi_{1-x}Mn_xO_3$

measurements on $SrTiO_3$ samples doped with Ni upto 0.8 at.% has been reported to be 1.01 and 1.03 eV, respectively [20, 21]. It has been reported from studies of conductivity as a function of partial pressure of oxygen that Ni-doped $SrTiO_3$ exhibits ionic conduction due to migration of doubly positively charged oxygen vacancies, $V_O^{\bullet\bullet}$. Values of activation energies of conduction obtained (Table 2) rule out possibility of intrinsic conduction in these materials. Value of E_a for $x = 0.01$ in the higher temperature range is greater than 1 eV and for $x = 0.05$ is close to 1 eV and seems to correspond to activation energy for diffusion of doubly positively charged oxygen vacancies/ions. Values of E_a for all other compositions in the high-temperature region are much less than 1.0 eV. In the lowest temperature region, values of E_a for compositions with $x \leq 0.30$ are almost equal and these decrease with increasing x. These values for $x \leq 0.30$ correspond to hopping of holes among Mn^{4+} and Mn^{3+} in the low-temperature range for all compositions and for $x = 0.50$, it corresponds to hopping of electrons among Mn^{2+} and Mn^{3+} ions. The activation energies for these samples in the intermediate temperature range are some what higher than that expected for hopping of charge carriers. This is because in this temperature range, E_a, also includes ionization energy of $V_O^{\bullet}$ which lies in the range 0.20–0.30 eV as mentioned earlier. Very high value of resistivity in the

Table 2 Activation energy, E_a, for DC conduction in the systems $Sr_{1-x}Gd_xTi_{1-x}Mn_xO_3$ and $Sr_{1-x}La_xTi_{1-x}Mn_xO_3$ and resistivity at 450 and 1,000 K of different compositions in the system $Sr_{1-x}Gd_xTi_{1-x}Mn_xO_3$

Composition	Temperature range (K)	Activation energy for (DC) $Sr_{1-x}Gd_xTi_{1-x}Mn_xO_3$ System (ev)	Temperature range (K)	Activation energy (DC) [8] $Sr_{1-x}La_xTi_{1-x}Mn_xO_3$ System (ev)	Temperature (K)	Resistivity for $Sr_{1-x}Gd_xTi_{1-x}Mn_xO_3$ system (ohm cm)
$x = 0.01$	400–600	0.50 ± 0.01	435–650	0.87 ± 0.01	450	2.181×10^{10}
	600–1,000	1.32 ± 0.01	650–1,000	1.37 ± 0.01	1,000	3.219×10^{4}
$x = 0.05$	345–630	0.42 ± 0.02	370–710	0.45 ± 0.01	450	2.025×10^{6}
	630–1,000	0.58 ± 0.01	710–1,000	0.88 ± 0.01	1,000	2.153×10^{3}
$x = 0.10$	300–1,000	0.39 ± 0.01	330–830	0.46 ± 0.01	450	4.751×10^{4}
			830–1,000	0.68 ± 0.01	1,000	1.655×10^{2}
$x = 0.30$	300–1,000	0.35 ± 0.02	300–560	0.36 ± 0.01	450	1.673×10^{4}
			560–620	0.39 ± 0.02	1,000	1.279×10^{2}
$x = 0.50$	300–465	0.19 ± 0.01	300–450	0.16 ± 0.01	450	1.236×10^{2}
					1,000	–

composition with $x = 0.01$ shows that compensation is almost complete in this composition. Value of α decreases continuously with temperature over the entire temperature range of measurements for compositions with $x \leq 0.10$, changing from positive to negative sign at high temperatures. For $x = 0.30$, α remains constant with temperature after becoming negative at high temperature, while it is negative and independent of temperature for $x = 0.50$ over the entire temperature range. Resistivity decreases with temperature over the entire temperature range for all the samples. Temperature-independent value of α and continuously decreasing value of ρ in the high temperature for $x = 0.30$ and over the entire temperature range for $x = 0.50$ indicate that the number of charge carriers is constant and mobilities are thermally activated in the regions mentioned for these samples. For $x < 0.10$, α keeps on decreasing even after temperature where it becomes negative. Therefore, for these samples, in this temperature range (Intermediate Temperature, IT), charge carriers are being generated due to ionization of singly ionized oxygen vacancies, $V_O^{\bullet}$ according to Eq. 12 and the mobilities are also thermally activated [22]. In these samples in the lower temperature region, (LT), conduction occurs by hopping of holes among Mn^{3+} and Mn^{4+}. This is supported by the observation that activation energy, E_a for DC conduction in the IT range is higher as compared to that in the lower temperature LT range. Electrical conduction behavior of this system is essentially similar to the analogous system $Sr_{1-x}La_xTi_{1-x}Mn_xO_3$ [8].

If one studies AC conductivity as a function of frequency and electrode polarization is absent, then one gets two plateaus and two dispersion regions [21]. The low-frequency plateau represents the total conductivity followed by a dispersion region in which grain boundaries contribution relaxes. This dispersion region is followed by a plateau which represents the contribution of grains to the total conductivity. The dispersion after this plateau in the highest frequency region represents the frequency dependence of bulk conductivity.

Plots of log σ_{ac} versus log f at a few selected steady temperatures and log σ_{ac} versus 1,000/T at a few selected frequencies for the compositions with $x = 0.01$, 0.10 and 0.50 are shown in Fig. 5(a–c) and (d–f), respectively. It is observed from Fig. 5a that for $x = 0.01$, two plateaus, one in the low-frequency region and other in the high-frequency range separated by a frequency-dependent region, are observed at 498 K. At 398 and 448 K, only one plateau in the low-frequency range followed by a frequency-dependent region is observed. Second high-frequency plateau is not observed at these temperatures. For $T \leq 398$ K, no distinct plateau is observed over the entire frequency range.

For compositions with $x = 0.10$ (Fig. 5b), a plateau followed by a frequency-dependent region is observed. Behavior of log of AC conductivity with temperature or frequency for composition with $x = 0.05$ (figure not shown) is similar to the composition with $x = 0.10$. The frequency range in which the second plateau occurs extends to higher frequency with increasing temperature. This represents the contribution of the grains to the total conductivity and the frequency-dependent region after this plateau represents the relaxation of the grain boundaries conductivity. The values of conductivity obtained from the plateau (as $f \rightarrow 0$) in these samples are almost equal to the corresponding values obtained by DC measurements in the same temperature range (Fig. 4). The plateau (in log σ_{ac} versus log f) extends to higher frequency range with increase in temperature. At the highest temperature, σ_{ac} remains constant over the entire frequency range.

Frequency dependent and very weak temperature-dependent AC conductivity is observed in the low-temperature region for all the compositions except the composition

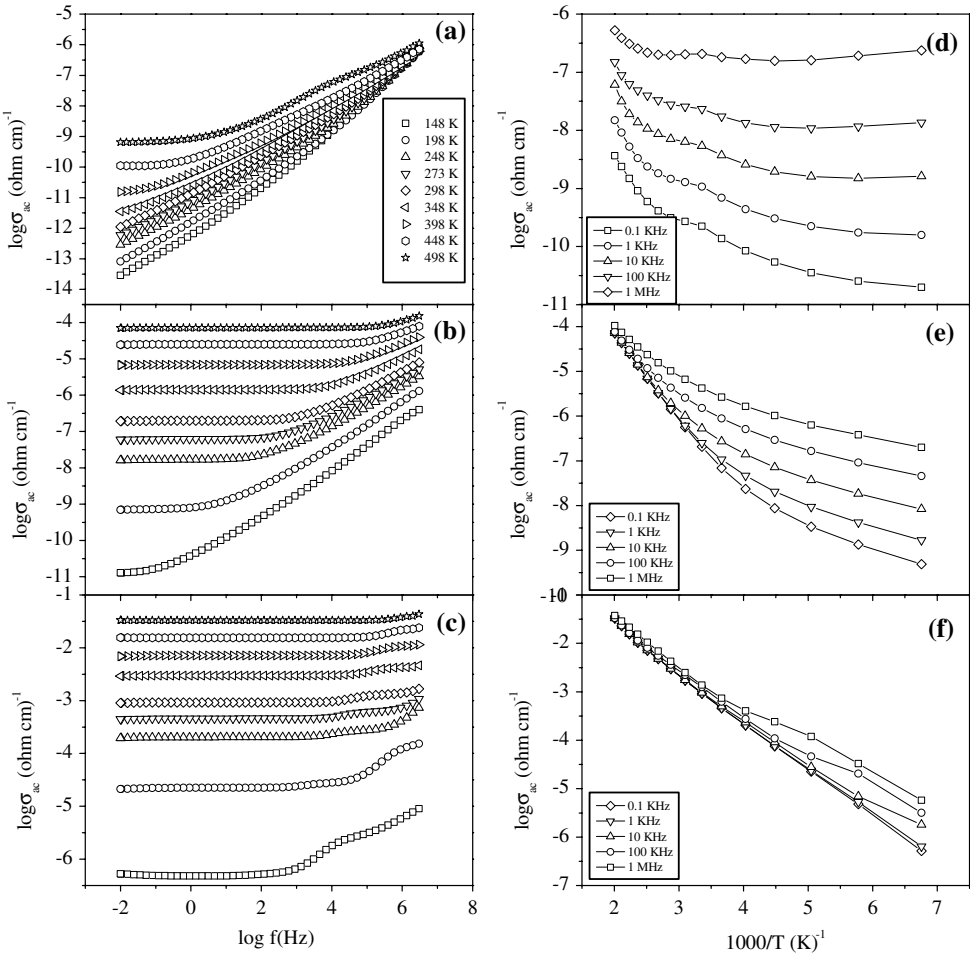

Fig. 5 Variation of log σ_{ac} with log frequency for the composition with x (**a**) 0.01, (**b**) 0.10 and (**c**) 0.50 and with inverse of temperature for the composition with (**d**) 0.01, (**e**) 0.10, and (**f**) 0.50 in the system $Sr_{1-x}Gd_xTi_{1-x}Mn_xO_3$

with $x = 0.50$ which exhibits significant temperature dependence in the low-temperature range (Fig. 5e). Variation of α with temperature for $x = 0.50$ is also different from other compositions as mentioned above. Frequency dependence decreases, but temperature dependence increases in the higher temperature range. A relaxation is observed in the intermediate temperature range in $x = 0.50$ at 10, 100 KHz and 1 MHz which moves to higher temperature with increase in frequency. Temperature dependence in the low-temperature region decreases with increasing frequency.

The frequency dependence of ac conductivity may arise due to the following mechanisms [23]:

(a) Transport by carriers excited to localized states near band edge and hopping at energy close to it. In this case, temperature dependence of σ_{ac} is given by

$$\sigma_{AC} \propto \exp[-(E_F - E_A)/kT] \quad (15)$$

(b) Hopping of charge carriers in the localized states near the Fermi level. For this case

$$\sigma_{AC} \propto T \quad (16)$$

if kT is small and independent of T if kT is larger than the bandwidth of defect band.

(c) Hopping of charge carriers among localized sites giving rise to a Debye-type loss similar to thermally activated rotation of dipoles. These dipoles can point out in two or more directions with different energies w_1 and w_2 ($\Delta w = w_1 - w_2$) and with jump time τ from lower to upper state. Both Δw and τ vary over a wide range, including zero

Here, $\sigma_{AC} \propto T$ if charge compensation is large and independent of T if charge compensation is small (17)

In polycrystalline ceramics, there are three contributions to the total observed resistance and capacitance. These are from grains (bulk), grain boundaries (GB) and electrode specimen interface. Each of these contributions can be represented as a parallel RC combination connected in series where R and C are the resistive and capacitive contributions of a particular contribution. The sample then corresponds to the three parallel RC combinations connected in series.

It is necessary to separate various contributions in order to understand the electrical behavior and tailor make it. Use is made of Immittance analysis for this purpose [24]. There are four Immittance functions viz. impedance Z^*, modulus

M^*, admittance Y^* and complex dielectric constant ε^*. We made use of Z^* and M^* which are given by:

$$\begin{aligned} Z^* &= Z' - iZ'' \\ M^* &= M' + iM'' \\ M' &= \omega C_o Z'' \\ M'' &= \omega C_o Z' \end{aligned} \tag{18}$$

where $\omega = 2\pi f$ is the angular frequency and C_o is capacitance of an empty cell. Z', M' and Z'', M'' represent the real and imaginary part of the respective functions. Immittance analysis is carried out in two ways (i) complex plane impedance or modulus analysis and (ii) impedance or modulus spectroscopy. In complex plane analysis, one measures Z', Z'', M' and M'' over a wide range of frequencies. Then imaginary part is plotted against the real part. One gets one, two or three circular arcs depending on whether all the three, two or only one contribution are present depending on the ratio of their time constants as well as relative magnitude of resistance and capacitance. In Z'' versus Z' plots, the intercepts of these arcs with real axis give contributions of resistance of corresponding part, viz. grains, R_g, grain boundaries, R_{gb} or electrode, R_e specimen interface. In M'' versus M' plot, the intercept on the real axis varies inversely with the capacitive contribution of that part. The value of resistance can be determined from the relationship $\omega RC = 1$ where ω is the angular frequency at highest point of arc and C is the capacitance of that contribution. The relaxation time τ for the process is given by $\tau = 1/\omega = RC$. If the relaxation process has a single value of $\imath = 1/\omega = RC$, then one observes a semicircular arc with its centre on the real axis. If there is a distribution of relaxation times, then one observes a depressed circular arc corresponding to that process. The angle that the line joining the centre of circle to the origin makes with real axis is a measure of distribution of relaxation times.

Second mode of analysis is known as immittance spectroscopic analysis. In this imaginary part of Immittance function (Z'' or M'') is plotted against log f. If the relaxation times for different processes occurring in the material are widely different, then one observes a peak corresponding to each process. The peak position gives the relaxation frequency. Height of the peak in Z'' versus log f plot is given by $R/2$, where R is the resistive contribution of that process. Height of the peak in M'' versus log f is given by $C_o/2C$, where C_o is capacitance of the empty cell and C is the capacitive contribution of the process. Complex plane plots are convenient to extract the value of capacitance and dc resistance of various contributions, while spectroscopic plots give the relaxation frequencies. Impedance and modulus plots give complementary information. Because of difference in the magnitude between resistive and capacitive contribution of grains and grain boundaries, grain boundaries' contribution is highlighted in the Z'' plots, while grains contribution is highlighted in the M'' plots. Hence Z'' and M'' spectroscopic plots give complementary information [24].

It has been shown that for a long-range process, peaks in Z'' and M'' versus log f plots will occur at the same frequency even for a very large relaxation ratio ($r = \varepsilon_s/\varepsilon_\infty$, where ε_s is the real permittivity when ω approaches zero and ε_∞ is the real permittivity when ω approaches infinity) while they will appear separately even for a small relaxation ratio [25] for conduction involving short-range migration of charge carriers. In the present case ε_s is taken as the value measured at lowest frequency (10^{-2} Hz/S) and ε_∞ is the value at the highest frequency (10^7 Hz/S). Thus by making use of complex plane impedance and modulus analysis along with impedance and modulus spectroscopy, one can separate the various contributions to the total.

Complex plane impedance plots for compositions with $x = 0.01$ and 0.10 are shown in Figs. 6 and 7, respectively. For compositions with $x = 0.01$, a steep line passing through the origin appears in Z'' versus Z' plots at temperatures $\leq$273 K. This is because of very high resistance of this sample in the low-temperature range. A partial circular arc passing through the origin is seen at 298 K. At higher temperature, two arcs are seen. Peak frequency determined from the corresponding Z'' versus log f plots is marked bold on the biggest arc appearing in these plots. Therefore this also represents relaxation frequency of one of the polarization processes. Because the resistance decreases with increasing x, the arcs start appearing in complex plane impedance plots of the compositions with $x \geq 0.05$ at low temperatures. One or two arcs are seen for all the samples depending on the temperature and their resistance. With increasing x and temperature, arcs are observed in the higher frequency range only.

By observing complex plane impedance and complex plane modulus plots (figure not shown) of various compositions, one can say that there are two relaxation processes in the samples. Generally contribution of electrode-sample interface to total resistance of a polycrystalline ceramic sample is small. If total resistance of the sample is sufficiently high this electrode—sample interface contribution can be neglected. The number of actual circular arcs appearing corresponding to these processes depends on the sample and temperature. Values of R's for grain and grain boundary processes are determined from the intercepts of the arcs with real axes (Z'). The logarithm of R_g and R_{gb} for all the compositions is plotted as a function of 1,000/T and activation energy of conduction is determined from the slopes of these Arrhenius plots. It has been found that grains and grain boundaries' process have almost equal value of

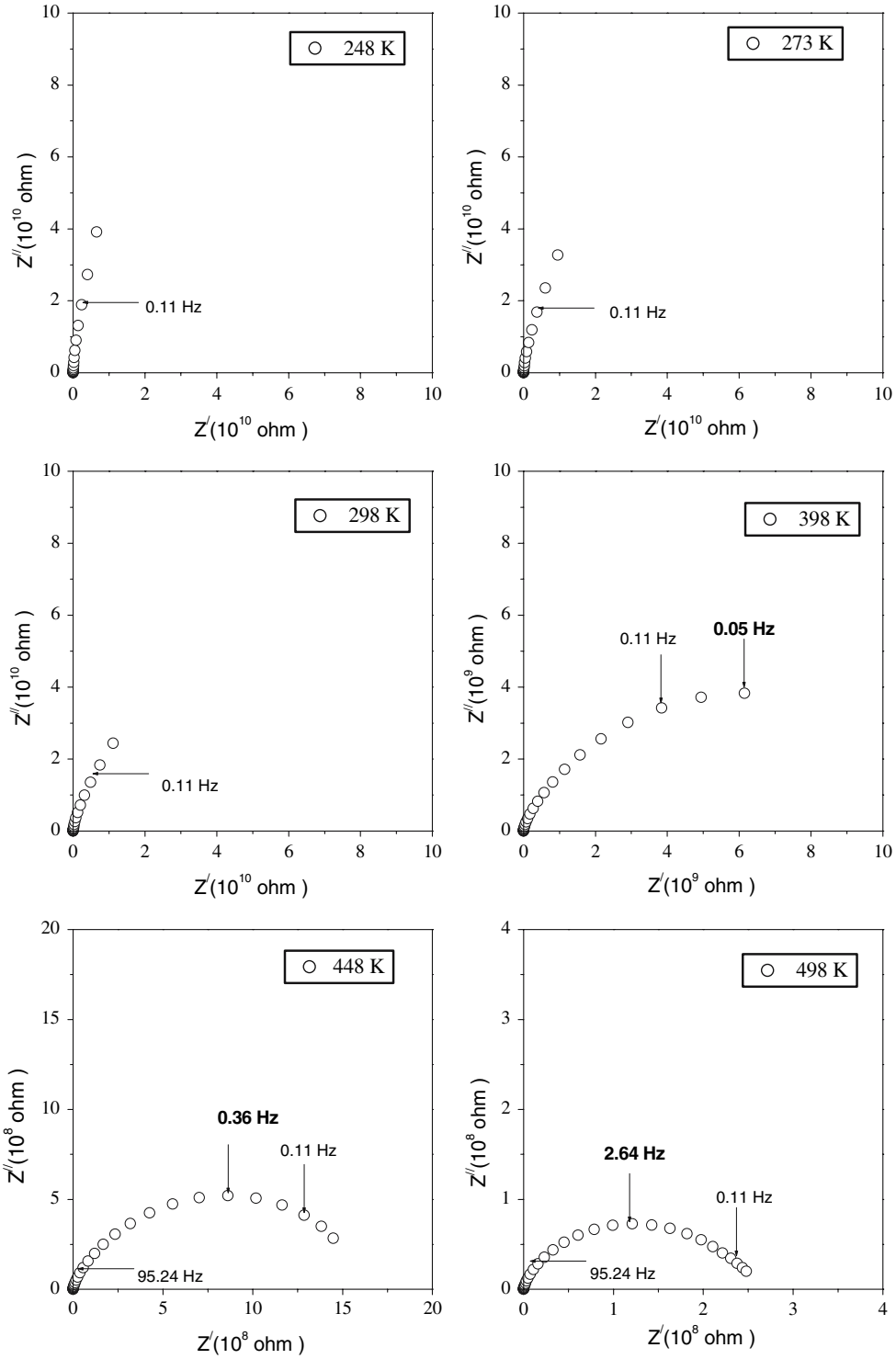

Fig. 6 Complex Plane Impedance (Z'' vs. Z') plots at a few selected temperatures for the composition $Sr_{0.99}Gd_{0.01}Ti_{0.99}Mn_{0.01}O_3$

activation energy, and this activation energy also matches with the activation energy determined from DC resistivity.

Plots of Z'' versus log f and M'' versus log f for compositions with $x = 0.01$, 0.30 and 0.50 are shown in Fig. 8. Z'' versus log f plots of the compositions with $x \leq 0.30$ are similar (Fig. 8a and b). A peak is seen in these plots. The temperature at which peak starts appearing decreases with increasing x. For $x = 0.50$ (Fig. 8c), an additional shoulder on the high-frequency side of peak at 148 K appears. The height of the peak in Z'' plots, which give $R/2$ where R is the resistance of the contributing polarization process, decreases with increasing temperature. This leads to decrease in the value of corresponding time constant, τ which shifts the relaxation frequency to higher

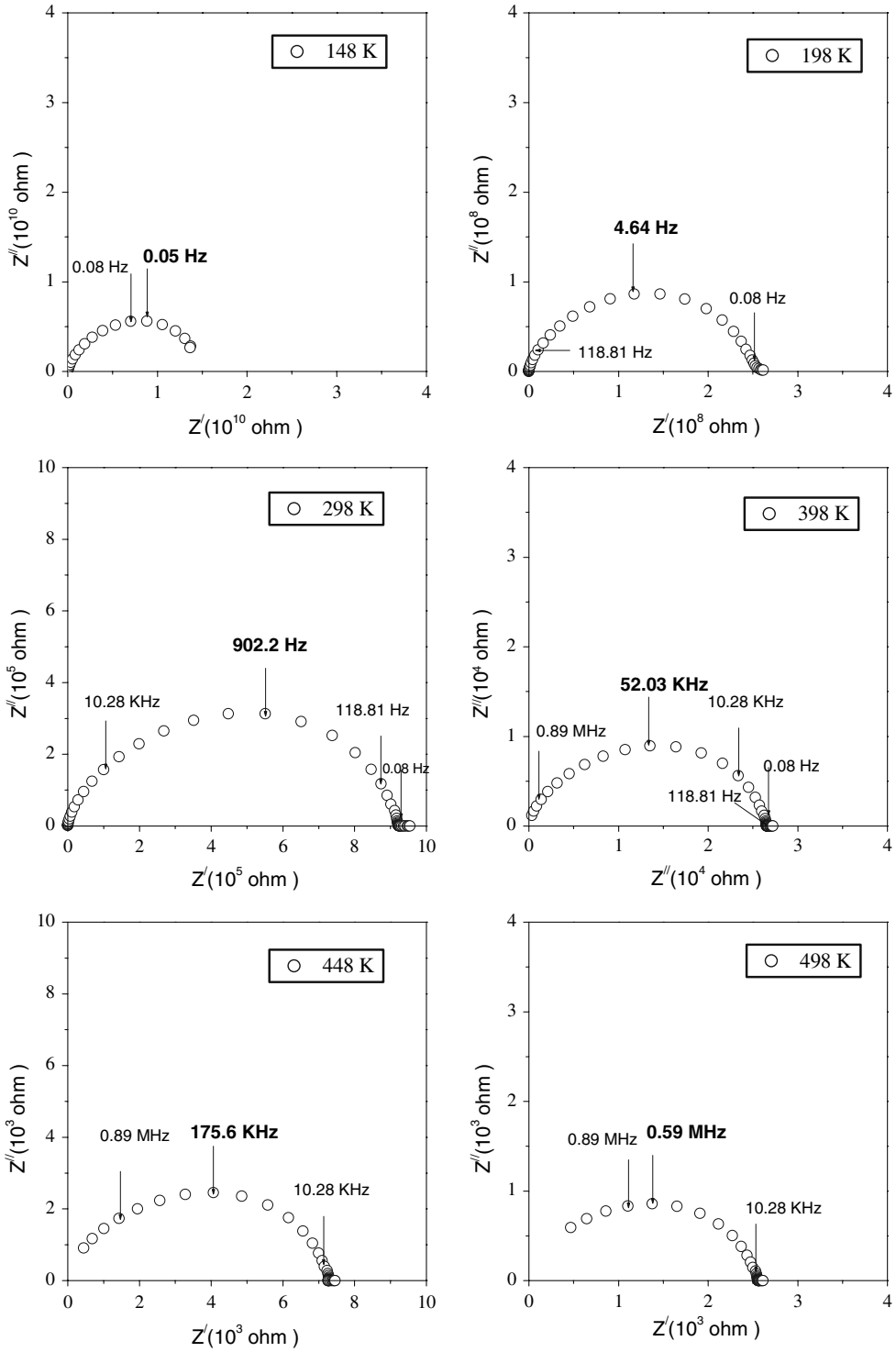

Fig. 7 Complex Plane Impedance (Z'' vs. Z') plots at a few selected temperatures for the composition $Sr_{0.90}Gd_{0.10}Ti_{0.90}Mn_{0.10}O_3$

temperature. Same effect is observed of increasing value of x on the temperature at which peak starts appearing in various compositions. With increase in x, the resistance decreases, leading to decrease in time constant, $RC = \tau$ and therefore the appearance of peak at higher frequency.

M'' versus log f plots of the compositions with $x \leq 0.10$ show an asymmetric peak with a long tail on the high-frequency side of the peak. The temperature, at which this peak starts appearing, decreases with increasing x. A shoulder is seen on the low-frequency side of the peak in the composition with $x = 0.30$ (Fig. 8e). For $x = 0.50$ (Fig. 8f), only one peak is observed at 148 K. At higher temperature, another peak may appear beyond frequency range of measurements. The height of the peak increases

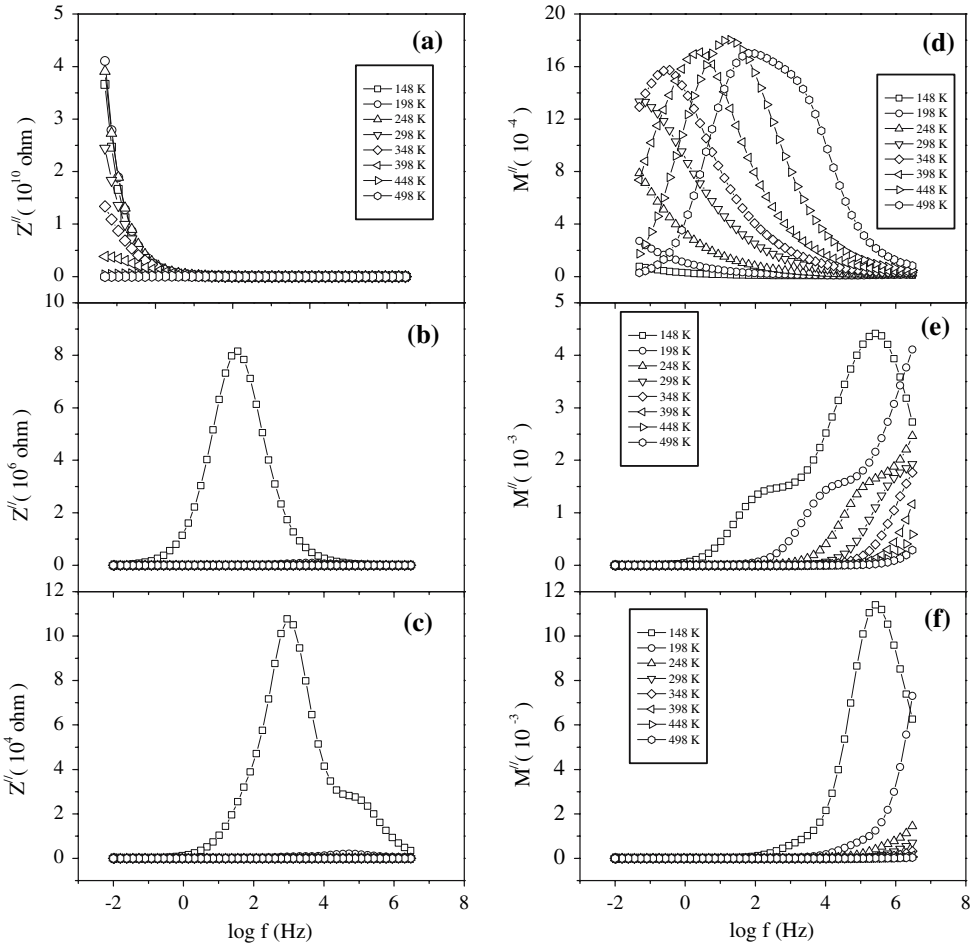

Fig. 8 Variation of Z'' with log f for the composition with x (**a**) 0.01, (**b**) 0.30 and (**c**) 0.50 and M'' with log f for the composition with (**d**) 0.01, (**e**) 0.30, and (**f**) 0.50 in the system $Sr_{1-x}Gd_xTi_{1-x}Mn_xO_3$

with increasing temperature except for the composition with $x = 0.01$ where it slightly decreases after 448 K. Increasing height with increasing temperature shows that capacitance decreases with temperatures. Full width at half maxima (FWHM) of both the peaks in Z'' and M'' versus log f plots are more than two decades indicating that they are summation of two relaxation processes.

Value of relaxation ratio r for various compositions in this system at a few selected temperatures is given in Table 3. From Table 3, it is observed that relaxation ratio r lies in the range 1.04–86.8 for all compositions. Combined plots Z'' and M'' versus log f for some compositions at a particular temperature are shown in Fig. 9. For $x = 0.30$, a shoulder on the lower frequency side coincides with the peak frequency in the Z'' plot (Fig. 9c). For $x = 0.50$ (Fig. 9d), the peak frequency in M'' plot seems to match with the peak frequency of the shoulder which appears on the higher frequency side of Z'' plot. From behavior of compositions with $x = 0.30$ and 0.50 (where one peak frequency in Z'' & M'' coincide), it is concluded that conduction occurs due to long-range migration of charge carries, i.e. electrons or holes among Mn^{2+}, Mn^{3+} and Mn^{4+}, Mn^{3+} respectively. For $x = 0.01$ and 0.10, second peak (contribution of grains) in Z'' versus log f plots seems to be suppressed due to higher resistance of grain boundaries as compared to grains.

Z'' peak occurring in the low-frequency range represents the grain boundaries' relaxation process because both R and C values are large in comparison to that of grains. M'' peak represents the grains relaxation process and occurs at higher frequencies. Peak frequencies are determined to calculate the relaxation times of grain and grain boundaries' processes. The logarithm of grains and grain

Table 3 Value of ratio ($\varepsilon_s/\varepsilon_\infty$) for various compositions in the system $Sr_{1-x}Gd_xTi_{1-x}Mn_xO_3$ at a few selected temperatures

Temperature (K)	Ratio ($\varepsilon_s/\varepsilon_\infty$) for system $Sr_{1-x}Gd_xTi_{1-x}Mn_xO_3$				
	$x = 0.01$	$x = 0.05$	$x = 0.10$	$x = 0.30$	$x = 0.50$
148	1.04	1.26	1.31	4.20	49.9
198	1.11	2.42	2.82	5.83	142
298	2.00	6.80	6.94	3.30	52.2
398	5.12	8.11	5.90	1.57	86.8
448	9.90	7.85	4.94	1.42	67.4
498	26.3	16.90	2.72	2.47	23.2

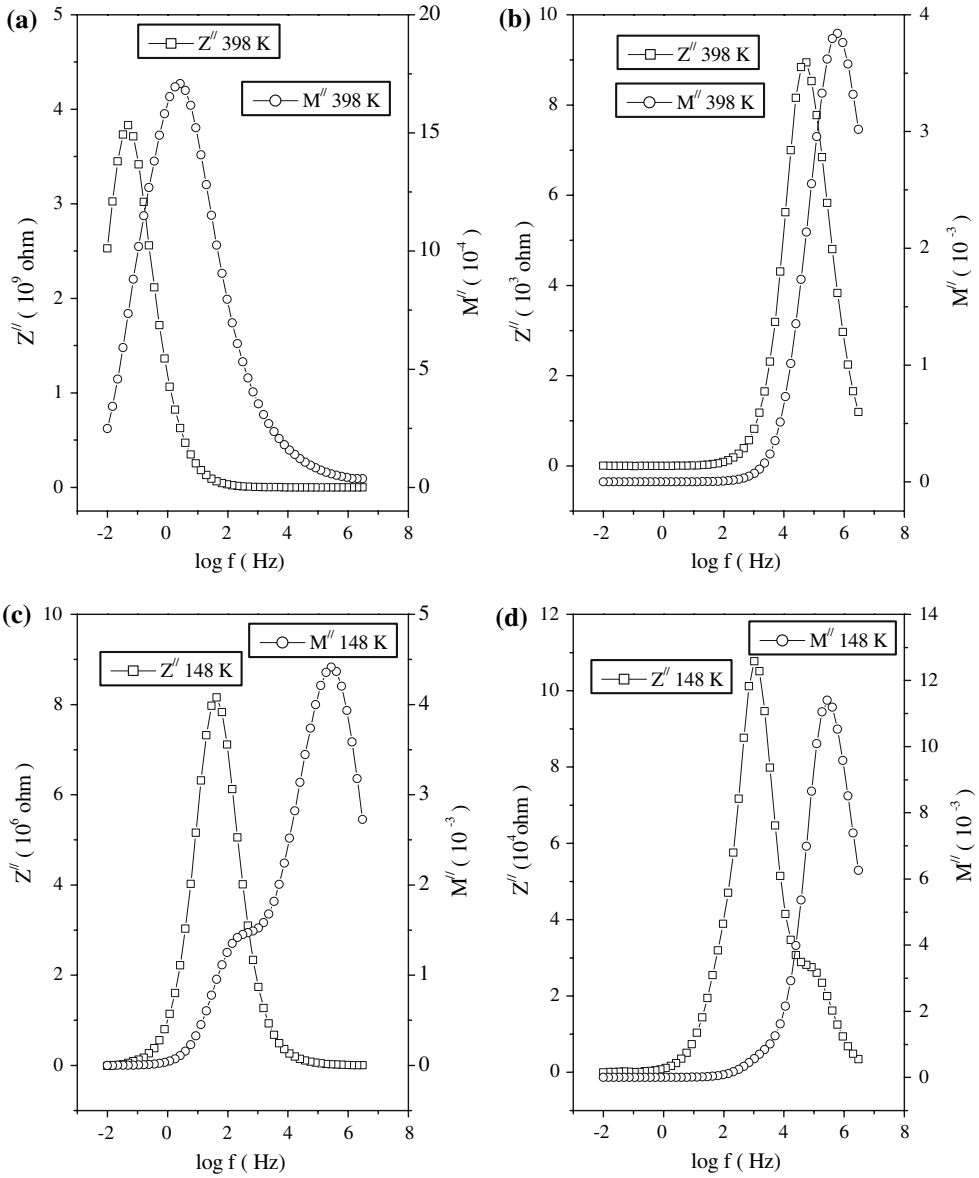

Fig. 9 Variation of Z'' and M'' with log f for the compositions with x (**a**) 0.01 (at 398 K), (**b**) 0.10 (at 398 K), (**c**) 0.30 (at 148 K), and (**d**) 0.50 (398 K) in the system $Sr_{1-x}Gd_xTi_{1-x}Mn_xO_3$

boundaries' relaxation time as determined from M'' versus log f and Z'' versus log f of different samples was plotted as a function of 1,000/T. From these plots, activation energies of the corresponding relaxation processes were determined. The values of activation energy for grains and grain boundaries relaxation in low- and high-temperature regions are given in Table 4. It has been found that both grain and grain boundary processes have similar activation energy, and this activation energy also matches with the activation energy for DC conduction in the low-temperature range. This corresponds to hopping of holes among Mn^{3+} and Mn^{4+} ions for $x \leq 0.30$ and hopping of electrons among Mn^{+2} and Mn^{+3} for $x = 0.50$ in the low temperature range. On comparing electrical conduction behavior of the system $Sr_{1-x}Gd_xTi_{1-x}Mn_xO_3$ with that of $Sr_{1-x}La_xTi_{1-x}Mn_xO_3$, it is found that the behavior of the two systems is essentially

Table 4 Activation energy of grain and grain boundary relaxation (E_g and E_{gb} respectively), determined using impedance and modulus spectroscopic plots for various compositions x in the system $Sr_{1-x}Gd_xTi_{1-x}Mn_xO_3$

Compositions (x)	Log τ_z versus 1,000/T plots		Log τ_m versus 1,000/T plots	
	E_{gb} (eV)		E_g (eV)	
	LT	HT	LT	HT
0.01	–	0.68	0.29	0.56
0.05	0.28	0.43	0.24	0.36
0.10	0.24	0.38	0.24	0.35
0.30	0.24	–	0.22	–
0.50	–	–	–	–

LT = low temperature, HT = high temperature

similar [8]. Presence of Gd in place of La does not significantly influence the electrical behavior. This may be because of complex nature of the system i.e., existence of manganese ions in different oxidation states whose concentration varies in a complex way with x.

Conclusions

Solid solution forms in all the compositions investigated. Crystal structure remains cubic, similar to $SrTiO_3$ for the compositions with $x \leq 0.10$ and it becomes orthorhombic similar to $GdMnO_3$ for $x \geq 0.30$ in the samples investigated. For $x = 0.01$, the conduction occurs in the higher temperature range due to migration of doubly positively charged oxygen vacancies. In the lower temperature range for all the compositions, it occurs due to hopping of charge carriers among localized sites (Mn^{2+}, Mn^{3+} and Mn^{4+}). At lower temperature, for x less than 0.30, conduction is dominated by hopping of holes among Mn^{4+} and Mn^{3+} ions, which are the majority charge carriers. With increase in temperature, conduction occurs due to hopping of electrons among Mn^{2+} and Mn^{3+} ions. Activation energy of conduction decreases with increasing x due to increase in the number of sites among which hopping takes place. Complex plane impedance plots of various compositions show that there are two relaxation processes in the samples. Electrical conduction behavior of this system is essentially similar to that of the previously reported $Sr_{1-x}La_xTi_{1-x}Mn_xO_3$ system.

Quenching the samples from higher temperature after annealing (>800 K) and studying their EPR and X-ray photoelectron spectra (XPS)as well as Seebeck coefficient and resistivity of quenched samples as a function of temperature will be useful in confirming the oxidation states of Mn and hence the mechanisms of conduction in different temperature ranges.

Acknowledgements We are thankful to Prof. K. Funke of Institut für Physikalische Chemie Westfälische Wilhelms Universität Münster, Germany, for providing low temperature facility. The authors are also grateful to Defence Research Development Organization, New Delhi, for providing financial support. Two authors are grateful to CSIR, New Delhi, for providing financial support.

References

1. Waku S (1967) Rev Elect Commun Lab 15:689
2. Yamaoka N, Masuyama M, Fukui M (1983) Bull Am Ceram Soc 62:698
3. Frederikse HPR, Thurber WR, Hosler WR (1964) Phys Rev A 134:442
4. Ravikumar V, Rodrigues RP, Dravid VP (1996) J Phys D Appl Phys 29:1799
5. Rodrigues RP, Chang H, Ellis DE,Dravid VP (1999) J Am Ceram Soc 82:2373
6. Rodrigues RP, Ellis DE, Dravid VP (1999) J Am Ceram Soc 82:2395
7. Shiqiang H, Anthony P (2002) Mat Res Bull 37:1215
8. Singh P, Parkash O, Kumar D (2006) J Appl Phys 99:123704
9. Ganguly P, Parkash OM, Rao CN (1976) Phys State Sol (a) 36:669
10. Mazadhyasni KS, Brown LM (1971) J Am Ceram Soc 54:539
11. Desu SB, Pyane AD (1990) J Am Ceram Soc 73:3398
12. Burn I, Neirman S (1982) Mater Sci 17:3510
13. Neirman S, Burn I (1984) J Mater Sci 19:737
14. Moos R, Menesklou W, Hardtl KH (1995) Appl Phys A 61:389
15. Moos R, Härdtl KH, (1996) J Appl Phys 80:393
16. Chan NH, Smyth DM (1976) J Electrochem Soc 123:1584
17. Mizushima K, Tanaka M, Iida S (1972) J Phys Soc Jpn 32:1519
18. Noland TA (1954) Phys Rev 94:724
19. Cardona M (1965) Phys Rev 140A:651
20. Vollmann M, Hagenbeck R, Waser R (1997) J Am Ceram Soc 80:2301
21. Waser R (1991) J Am Ceram Soc 74:1934
22. Karim DP, Aldred AT (1979) Phys Rev B 20:2255
23. Mott NF, Davis EA (1979) Electronic processes in non-crystalline materials, Chapter 6. Clarenden, London
24. Hodge IM, Ingram MD, West AR (1976) J Electro Anal Chem 74:125
25. Gerhardt R (1994) J Phys Chem Solids 55:1491